# Improving the Representation of Resolved and Unresolved Topographic Effects on Surface Wind in the WRF Model

PEDRO A. JIMÉNEZ

*División de Energías Renovables, CIEMAT, Madrid, Spain, and Mesoscale and Microscale Meteorology Division, National Center for Atmospheric Research,* Boulder, Colorado*

JIMY DUDHIA

*Mesoscale and Microscale Meteorology Division, National Center for Atmospheric Research,* Boulder, Colorado*

(Manuscript received 19 April 2011, in final form 13 October 2011)

ABSTRACT

The Weather Research and Forecasting (WRF) model presents a high surface wind speed bias over plains and valleys that constitutes a limitation for the increasing use of the model for several applications. This study attempts to correct for this bias by parameterizing the effects that the unresolved topographic features exert over the momentum flux. The proposed parameterization is based on the concept of a momentum sink term and makes use of the standard deviation of the subgrid-scale orography as well as the Laplacian of the topographic field. Both the drag generated by the unresolved terrain and the possibility of an increase in the speed of the flow over the mountains and hills, where it is herein shown that WRF presents a low wind speed bias, are considered in the scheme. The surface wind simulation over a complex-terrain region that is located in the northeast of the Iberian Peninsula is improved with the inclusion of the new parameterization. In particular, the underestimation of the wind speed spatial variability resulting from the mentioned biases is corrected. The importance of selecting appropriate grid points to compare with observations is also examined. The wind speed from the nearest grid point is not always the most appropriate one for this comparison, nearby ones being more representative. The new scheme not only improves the climatological winds but also the intradiurnal variations at the mountains, over which the default WRF shows limitations in reproducing the observed wind behavior. Some advantages of the proposed formulation for wind-resource evaluation are also discussed.

## 1. Introduction

The Weather Research and Forecasting (WRF) model (Skamarock et al. 2008) has presented a high surface wind speed bias over land since the early versions of the model (Cheng and Steenburgh 2005). The bias still persists in more recent versions (e.g., Bernardet et al. 2005; Roux et al. 2009; Mass and Ovens 2010, 2011) and represents a limitation for the high demand of accurate surface wind estimations by different sectors such as wind-energy applications or air-quality studies.

A plausible explanation for the high bias could be the smoother topography used in the model to simulate the atmospheric evolution. It could be argued that the unresolved topographic features produce an additional drag to that generated by vegetation. If their effects are not considered, such as is the case for WRF, it can lead to an overestimation of the wind speed. Indeed, the effects produced by unresolved orographic features have been considered in other atmospheric models, revealing improvements in the model performance (Mesinger et al. 1996; Milton and Wilson 1996; Georgelin et al. 2000; Rontu 2006).

The effects that the unresolved topography exerts over momentum fluxes have been parameterized according to two different concepts. The first makes use of an *effective roughness length* (Fiedler and Panofsky 1972) to take into

* The National Center for Atmospheric Research is sponsored by the National Science Foundation.

*Corresponding author address:* Pedro A. Jiménez, Mesoscale and Microscale Meteorology Division, National Center for Atmospheric Research, 3450 Mitchell Ln., Boulder, CO 80301.
E-mail: jimenez@ucar.edu

DOI: 10.1175/JAMC-D-11-084.1

account the additional drag generated by the topographic features. It is based on the idea that the area-averaged wind profile follows the logarithmic wind profile in a way that is similar to the way that turbulence does, but replacing the vegetative roughness length $z_0$ by the effective roughness length $z_{\text{eff}}$, which is a function of the terrain complexity (Grant and Mason 1990; Wood and Mason 1993). Parameterizations based on this concept have been implemented in several numerical models, showing positive effects such as a realistic reduction of the mountain wave amplitude (Georgelin et al. 2000).

The second group of parameterizations is based on the works of Wood et al. (2001) and Brown and Wood (2001), who proposed the representation of the drag generated by the subgrid-scale orography by introducing a sink term in the momentum equations. The idea is also supported by the theoretical study of Wilson (2002) that mathematically showed that the effects of the unresolved orography can be represented by the sink term. The form of the extra term has been deduced from theoretical studies of flows over hills and a considerable number of assumptions that cannot always be justified (Beljaars et al. 2004; Rontu 2006). Parameterizations following this approach present certain advantages over those that are based on the effective roughness length. For instance, sink-term-based approaches do not impose any additional restriction on the location of the lowest model level whereas the $z_{\text{eff}}$-based approaches need to satisfy $z_{1\text{st\_level}} \gg z_{\text{eff}}$ instead of $z_{1\text{st\_level}} \gg z_0$, which logically reduces the potential locations of the first level. Another disadvantage is that schemes using $z_{\text{eff}}$ need to compensate the effects that the increase in the roughness length produces on heat- and moisture-related processes (Beljaars et al. 2004). Other schemes enhance the friction velocity $u_*$ instead of $z_0$ (Chien and Mass 1994), but this approach still suffers from limitations that are similar to those of the $z_{\text{eff}}$-based approaches.

The purpose of this work is to develop a new parameterization to represent the subgrid-scale orographic effects over momentum to correct the high wind speed bias of the WRF model. The proposed parameterization modulates the intensity of the surface drag in the momentum equation according to the terrain characteristics. Hence, it follows the philosophy of representing the effects of the unresolved orography with a sink term. The scheme not only allows for representing the drag associated with the unresolved orography but also improves the model representation of the increase in speed of the flow over the tops of hills or mountains. This has been shown to improve the diagnosis of the wind speed estimations from mesoscale models (Howard and Clark 2007) but to our knowledge has not been implemented before in a mesoscale model.

The scheme has been tested against wind observations taken over the Comunidad Foral de Navarra (CFN), a complex-terrain region that is located in the northeast of the Iberian Peninsula (Fig. 1). The existence of wind data of quality (Jiménez et al. 2010b), as well as a distribution of stations that covers a wide range of locations (valleys, plains, mountain and hill tops, etc.), converts the area into an excellent framework for the specific purposes of this investigation.

An additional advantage of the CFN is the existence of a WRF simulation performed by Jiménez et al. (2010a) at a high horizontal resolution (2 km) during the 1992–2005 period. Jiménez et al. (2010a, hereinafter JEA10) have shown the ability of the simulation to reproduce the observed wind variability over the area (Jiménez et al. 2008). The research presented here will use the JEA10 simulation to evaluate WRF's ability to reproduce the climatological wind speeds and therefore complements in certain ways the results of JEA10. A relevant aspect for this investigation is the finding in JEA10 that the nearest grid point is not necessarily the most representative of the wind characteristics of a given location, nearby grid points being more appropriate. Following JEA10, this will be referred to as the representativeness error. The reason for this kind of comparative problem relies on the spatial discretization inherent to any atmospheric model that smooths the surface physical properties such as orography or land-use characteristics. It will be herein shown that the combination of the parameterization of the unresolved terrain features and the selection of representative grid points leads to significant improvements in the surface wind speed estimations.

The rest of the article is organized as follows. The next section describes the observational dataset and uses the JEA10 simulation to provide what can be considered to be the rationale for parameterizing the effects of the unresolved terrain features. Section 3 explains the parameterization, and section 4 describes the numerical experiment performed to test its performance. The results are presented in section 5, and section 6 contains a summary with a discussion of the study and the conclusions.

## 2. The necessity to parameterize unresolved topographic effects

### *a. Observational evidence*

The location of the CFN within the Iberian Peninsula is shown in Fig. 1. The area is dominated by the presence of the western ridges of the Pyrenees in the north and the plains of the broad Ebro valley in the south (see zoomed-in area in Fig. 1). As a consequence, the topography is more complicated in northern areas of the

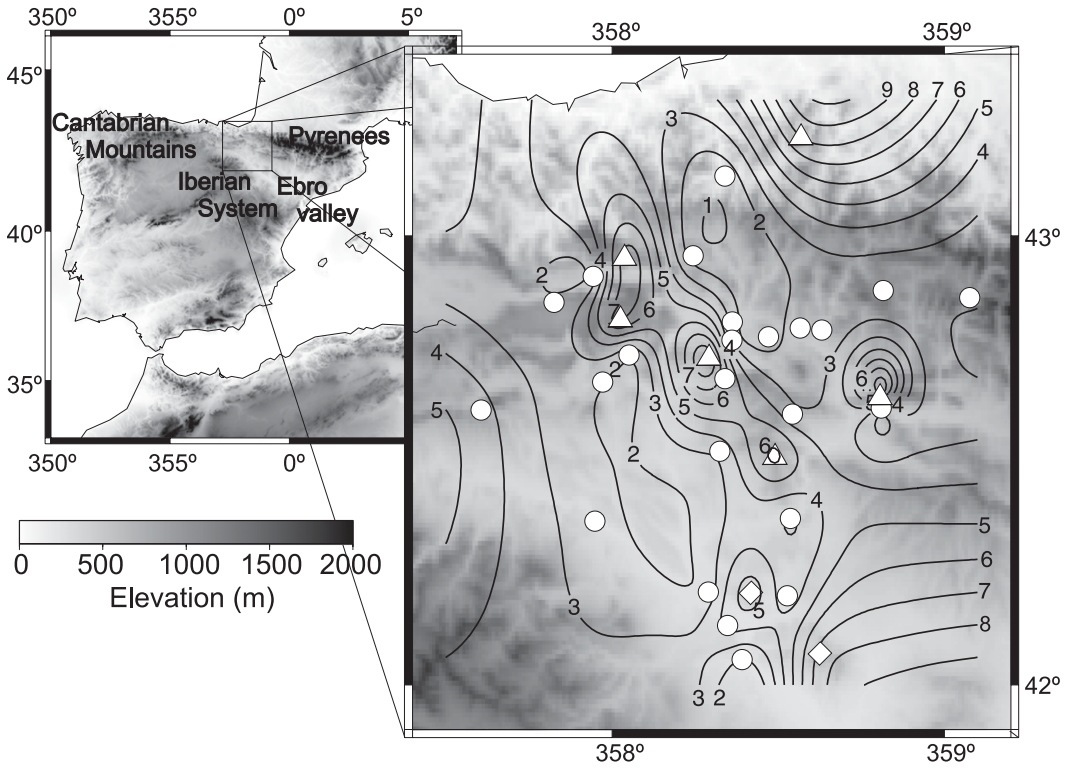


FIG. 1. Location of the area of study within the Iberian Peninsula. The symbols in the zoomed-in area represent the locations of the observational sites. Sites located at mountaintops and hills are represented with triangles and diamonds, respectively. The contour lines represent the mean wind speed (m $s^{-1}$) calculated with observations spanning the 1992–2005 period (Jiménez et al. 2010b).

region than in the south, where the terrain is mostly flat, excluding a few hills. These characteristics of the region can be better appreciated in Fig. 2, which clearly shows the topographic contrast between northern and southern areas of the CFN.

A total of 32 observational sites with wind speed measurements recorded at 10 m above ground level are used in this investigation. The locations of the observational sites and the codes of the stations are also shown in Fig. 2. The observational network provides good spatial coverage, sampling many important locations that are representative of the topographic characteristics of the CFN. For instance, stations in southern areas are not only located over the plains but also over the hills (stations 7 and 8). There are also stations located over narrow and complicated valleys in the Pyrenees (22 and 29) or in northern areas (15 and 26) and stations in more gentle valleys such as those to the south of the Pyrenees (e.g., 2, 10, 18, 21, 27, and 41). In addition to the stations located over valleys, plains, and hills, there are a total of six stations placed at mountaintops (3, 4, 16, 20, 35, and 37). Few studies have evaluated the wind at these extreme locations (e.g., Rife et al. 2009, JEA10).

The wind observations taken during the period from 1992 to 2005 have been subjected to a quality-control process to remove the most important inconsistencies in the records (Jiménez et al. 2010b). The quality-controlled wind observations have been used to investigate very different characteristics of the surface circulations in this region (e.g., Jiménez et al. 2008, 2009a, 2011; García-Bustamante et al. 2012). For instance, Jiménez et al. (2009a) have shown the strong influence that topography produces by channeling the synoptic flow. The mean wind speed is shown in Fig. 1. The wind is higher at the sites located at mountaintops and at the two stations located on top of hills in the southern plains. The stations over the valleys reveal a lower wind speed, especially in the northern areas where the complexity of the orography is higher. The climatological wind speeds therefore reveal a strong dependence on the specific terrain characteristics of the region.

### b. Numerical evidence

The wind speed bias of the WRF simulation performed by JEA10 (1992–2005 period) is shown in Fig. 3a. The observations (10 min) and the WRF output (1 h) were

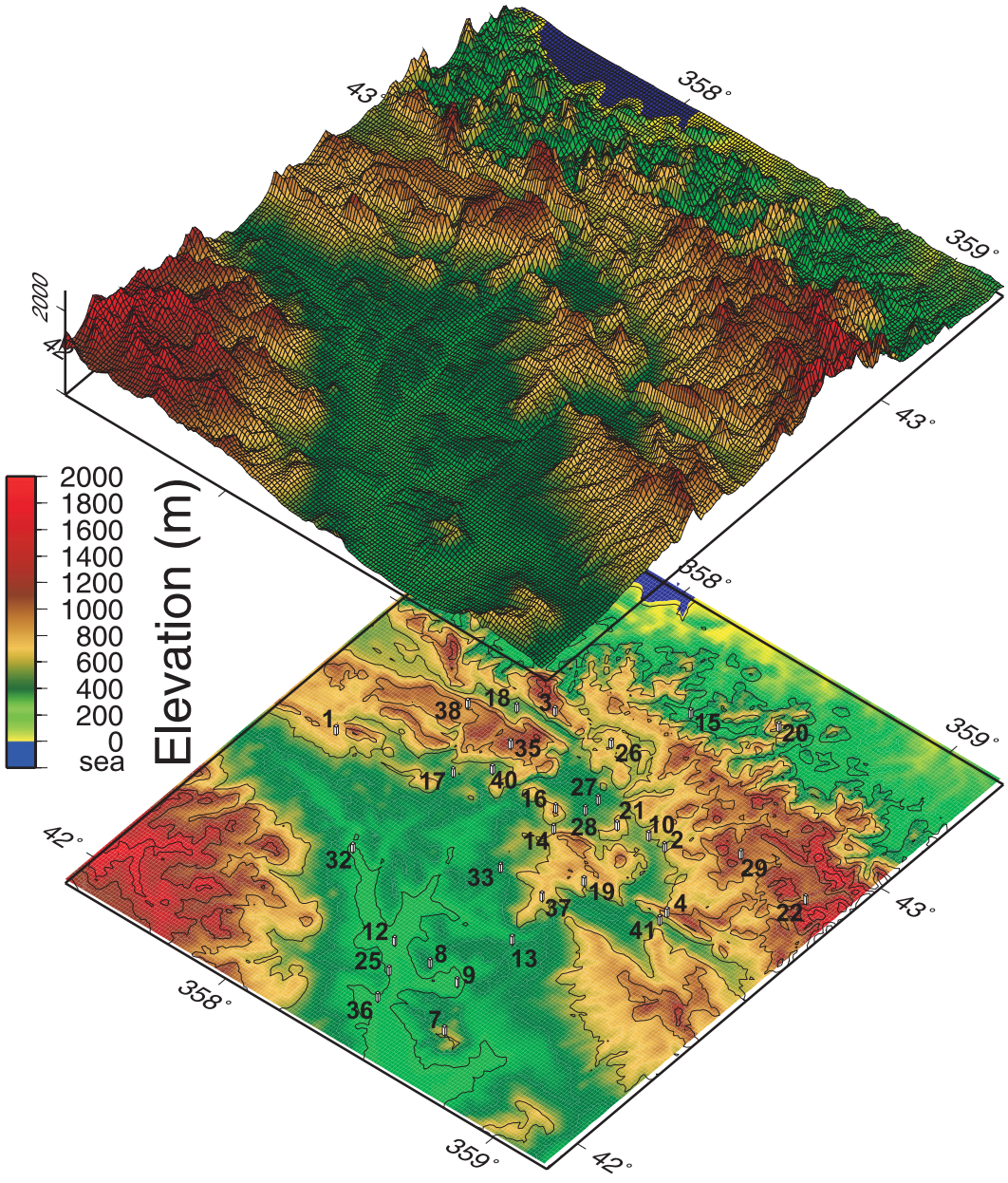


FIG. 2. (top) Topographic features of the CFN, with slopes exaggerated by a factor of 10. (bottom) The locations of the observational sites together with their codes, as in Jiménez et al. (2010b).

daily averaged (JEA10) before computing the long-term bias. There is a tendency for the simulation to underestimate the wind speed at the observational sites located at hills and mountaintops, which are the windiest sites, and to overestimate the wind speed at the locations situated in the plains and in the valleys, the less-windy areas. This result can be better appreciated in Fig. 3b, which displays the dispersion diagram of the mean wind speed versus the wind speed bias. Locations with low (high) wind speed show a positive, or high, (negative, or low) bias. This result reveals that WRF underestimates the wind speed spatial variability.

The mean wind speed bias is 0.06 m $s^{-1}$, indicating that the high bias over the valleys and plains (1.06 m $s^{-1}$) is compensated by the low bias at the hills and mountains (−2.93 m $s^{-1}$). This result suggests that the high wind speed bias reported by previous studies (e.g., Bernardet et al. 2005; Roux et al. 2009; Mass and Ovens 2010, 2011) may be a consequence of the uneven sampling of the wind by the meteorological networks, which

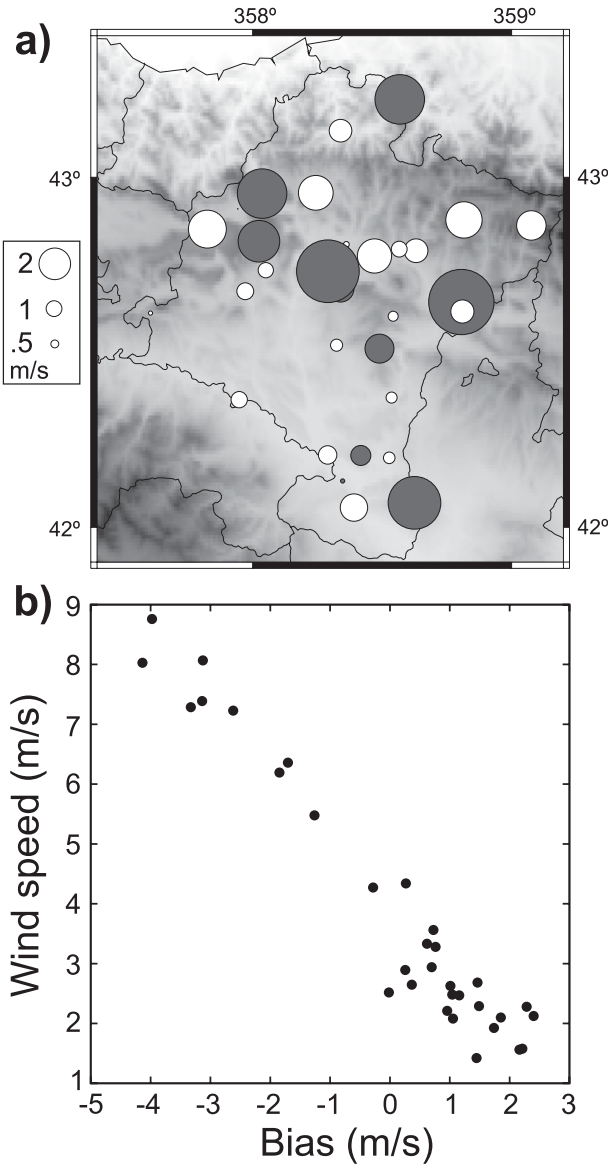


FIG. 3. (a) Wind speed bias calculated with the JEA10 simulation. The white (dark gray) color denotes a high, or positive, (low, or negative) bias. (b) The scatter diagram of the wind speed bias vs the mean observed wind speed.

tend to represent more stations over plains and valleys than over mountains or hills.

The different behavior that the simulation shows in reproducing the climatological wind speed at plains/valleys and at mountain locations could stem from the smoother topography within the mesoscale model. It could be argued that even the high horizontal resolution used by JEA10 (2 km) is not able to represent with enough accuracy the complexity of the terrain over the CFN. This misrepresentation can potentially introduce systematic errors to the simulation, which ultimately would lead to the wind speed overestimation (underestimation) at the valleys and plains (mountaintops and hilltops).

A plausible explanation for the wind speed overestimation at the plains and valleys could be the drag generated by the unresolved orography, whose effects have been shown to be of relevance for surface wind simulation (e.g., Beljaars et al. 2004; Rontu 2006; Howard and Clark 2007) and are not parameterized in WRF. According to this interpretation, the wind speed overestimation would be higher at the locations with more complex terrain at which the unresolved drag due to the subgrid-scale orography would be higher. This seems to be the case in this simulation in which the wind speed overestimation is higher at the sites located in the areas with more complex terrain in the north of the region than at the smoother plains in the south (Fig. 3a). To inspect this possibility, a more-realistic-terrain dataset of 90-m resolution (Farr et al. 2007; Reuter et al. 2007) is used to explore the characteristics of the unresolved topography.

Figure 4 shows the standard deviation of the subgrid-scale orography $\sigma_{sso}$ within each grid cell (2 km). The standard deviation provides an idea of the variability and, thus, the complexity of the terrain. As expected, the northern areas of the CFN show a higher variance of the unresolved terrain, conferring more credibility to the attribution of the high bias to the absence of a topographic drag in WRF. This is better appreciated in Fig. 5a, which shows the dispersion diagram between the wind speed bias and $\sigma_{sso}$ and confirms that the high bias (plains and valleys) increases with terrain complexity. This indicates that the wind speed bias in the plains and valleys is consistent with the exclusion of the subgrid-scale topography in the WRF simulation.

Another aspect of the simulation that can be extracted from Fig. 5a is that sites located at hills or mountaintops (low bias) also present a direct relationship between the bias and $\sigma_{sso}$. A high $\sigma_{sso}$ within a grid cell located over a mountaintop could be indicative of a steep peak. Hence, the results could be suggesting that the steeper the peak is, the larger is the magnitude of the low bias. On the other hand, a sharp peak inevitably would lead to an underestimation of its height by WRF (at least at the usual horizontal resolutions). If one keeps in mind that the wind increases with height in the lower troposphere and one assumes that the mountaintops are well exposed to this geostrophic wind, a plausible explanation for the wind speed underestimation at the mountaintops could be WRF's representation of mountains that are flatter than the actual mountains. This seems to be the case in the JEA10 simulation since, even at the high horizontal resolution used (2 km), the mountains are considerably

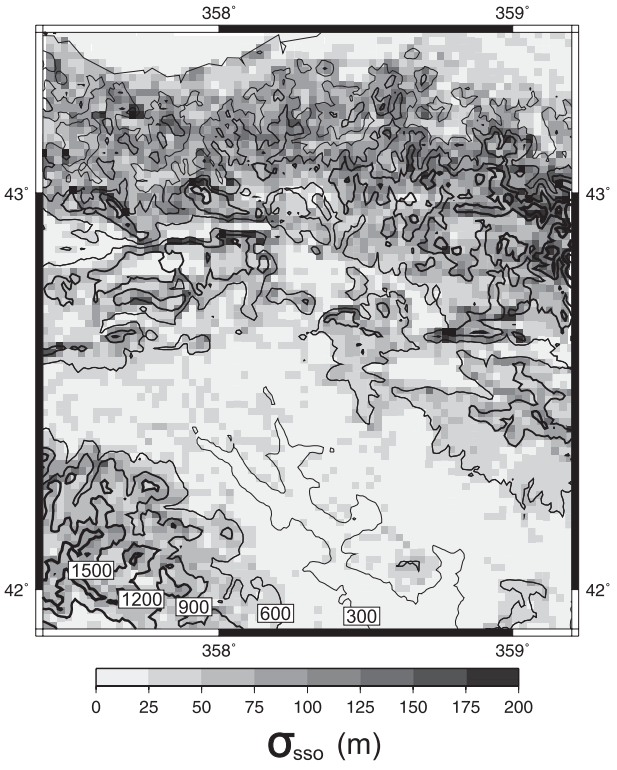


FIG. 4. Standard deviation of the subgrid-scale orography $\sigma_{sso}$ (shaded), calculated using a high-resolution-terrain dataset (Farr et al. 2007; Reuter et al. 2007) and the grid cells defined in the JEA10 simulation. The topography is also shown (contour lines).

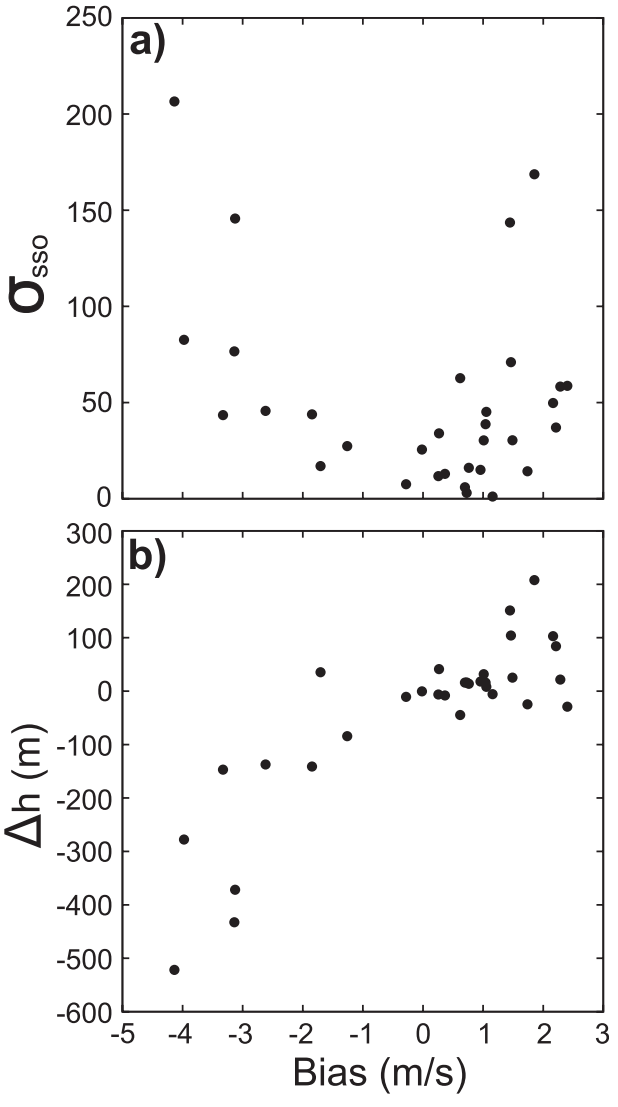


FIG. 5. (a) Standard deviation of the subgrid-scale orography vs the wind speed bias, and (b) topographic difference between the elevation of the stations and the topography used in WRF vs the wind speed bias.

smoother than reality (−452, −521, −277, −371, −137, and −141 m for stations 3, 4, 16, 20, 35, and 37, respectively). The interpretation becomes more evident by representing the wind speed bias versus the topographic differences between the terrain height used in the simulation (2 km) and the true elevation of the stations. The comparison is displayed in Fig. 5b. The stations at hills and mountaintops (i.e., sites with a low bias) show an increased magnitude of the bias as the terrain differences increase, suggesting that the wind speed underestimation is accentuated with increasing underestimation of the mountain heights. Therefore, the low wind speed bias is also consistent with deficiencies in the terrain representation.

The problem at mountaintop locations is even worse since the simulation not only is unable to reproduce the mean wind but also produces a wind diurnal cycle of opposite phase to that observed (Jiménez et al. 2009b). Figure 6 shows the diurnal wind speed cycle as a result of averaging the observations/simulation from 1992 to 2005 at station 20. The observations show a wind speed minimum (maximum) during the day (night) whereas the simulation shows the opposite behavior. The wind speed diurnal cycle at the first model level (instead of the one diagnosed at 10 m above ground level) is also shown in Fig. 6. Although it still shows discrepancies, it is in better agreement with the observed diurnal cycle. In particular, the mean wind estimation is improved, but more important than this is that it shows changes in the diurnal evolution that go in the correct direction toward the tendency of the observations to show a minimum wind during the day. Similar behavior has been found at the other mountain sites where observations are available (Fig. 1). The wind speed at the mountain sites is actually in better agreement with the upstream flow at its elevation than with the diagnosed surface wind, which suggests

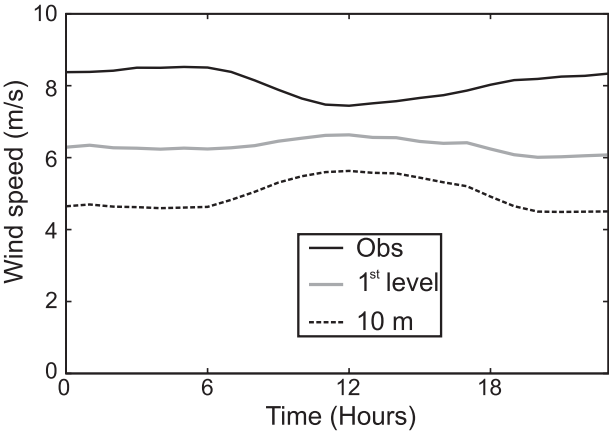


FIG. 6. Wind speed diurnal cycle at station 20 calculated with observations (black solid line) and the wind at the first model level (gray solid line) and 10 m above ground level (dashed line) from the JEA10 simulation. Both the observations and the simulation span the 1992–2005 period.

that the flow at these sites is in certain ways decoupled from the local effects of the ground.

## 3. Parameterization of the topographic effects

An important characteristic of the proposed formulation is that it distinguishes between plains/valleys and mountains/hills to introduce appropriate corrections for the specific problems encountered at these sites (see previous section). The differentiation has been accomplished by applying the following operator to the topographic field $h$:

$$\Delta^2 h_{i,j} = 0.25(h_{i+1,j} + h_{i,j+1} + h_{i-1,j} + h_{i,j-1} - 4h_{i,j}), \quad (1)$$

which we will call hereinafter the nondimensional Laplacian operator and is related to the traditional Laplacian by $\nabla^2 h = \Delta^2 h/(\Delta x)^2$. Positive values indicate the presence of a minimum (a valley), and negative values denote a maximum (hills or mountains); near-zero values are indicative of plains. The nondimensional Laplacian operator is independent of the horizontal resolution and therefore confers more flexibility on the definitions that follow.

The nondimensional Laplacian of the topography $\Delta^2 h$ calculated with the WRF simulation of JEA10 is shown in Fig. 7a. The topography is also shown (contour lines). The quantity $\Delta^2 h$ clearly identifies whether a particular grid cell is a valley (positive values) or a hill/mountain (negative ones). To implement the parameterization in WRF, a threshold value of $-20$ m has been selected to classify the individual grid cells. Cells with $\Delta^2 h > -20$ m are defined as valleys/plains and those with $\Delta^2 h < -20$ m are hills/mountainous areas. The adequacy of this definition can be inspected in Fig. 7b, which shows how grid cells with $\Delta^2 h < -20$ m are indeed located over the mountains/hills.

The effects of the unresolved terrain have been parameterized, introducing a factor $c_t$ that stands for the correction for topography and modulates the surface drag associated with vegetation in the momentum-conservation equation:

$$\frac{\partial u}{\partial t} = \cdots - c_t \frac{u_*^2}{\Delta z} \frac{u}{V}. \quad (2)$$

Here $u$ stands for the zonal wind component at the first model level, $V$ is the wind speed—also at the first model level, $u_*$ is the friction velocity that comes from the surface-layer scheme, and $\Delta z$ is the thickness of the first model layer. An analogous modification is also introduced for the meridional wind equation. The factor $c_t$ is equal to 1 in the default WRF model. Here, $c_t$ is a function of the terrain characteristics. In physical terms, it can be interpreted as the modifications that orography produces over the friction velocity calculated assuming homogeneous terrain. The factor $c_t$ is a function of $\Delta^2 h$ and $\sigma_{\text{sso}}$:

$$c_t = \begin{cases} 1 & \text{if} \quad \Delta^2 h > -20 \quad \text{and} \quad \sigma_{\text{sso}} < e \\ \ln\sigma_{\text{sso}} & \text{if} \quad \Delta^2 h > -10 \quad \text{and} \quad \sigma_{\text{sso}} > e \\ \alpha \ln\sigma_{\text{sso}} + (1 - \alpha) & \text{if} \quad -10 > \Delta^2 h > -20 \quad \text{and} \quad \sigma_{\text{sso}} > e \\ \dfrac{\Delta^2 h + 30}{10} & \text{if} \quad -20 > \Delta^2 h > -30 \\ 0 & \text{if} \quad -30 > \Delta^2 h \end{cases},$$

with $\alpha = (\Delta^2 h + 20)/10$ and $e$ being the natural logarithm base (2.718). In basic terms, $\Delta^2 h$ corrects for the low bias over steep mountaintops by decreasing the drag to zero as these tops become sharper (Fig. 8a). This decision is supported by the decoupling of the flow from the surface effects that seem to occur at mountain sites (see Fig. 6

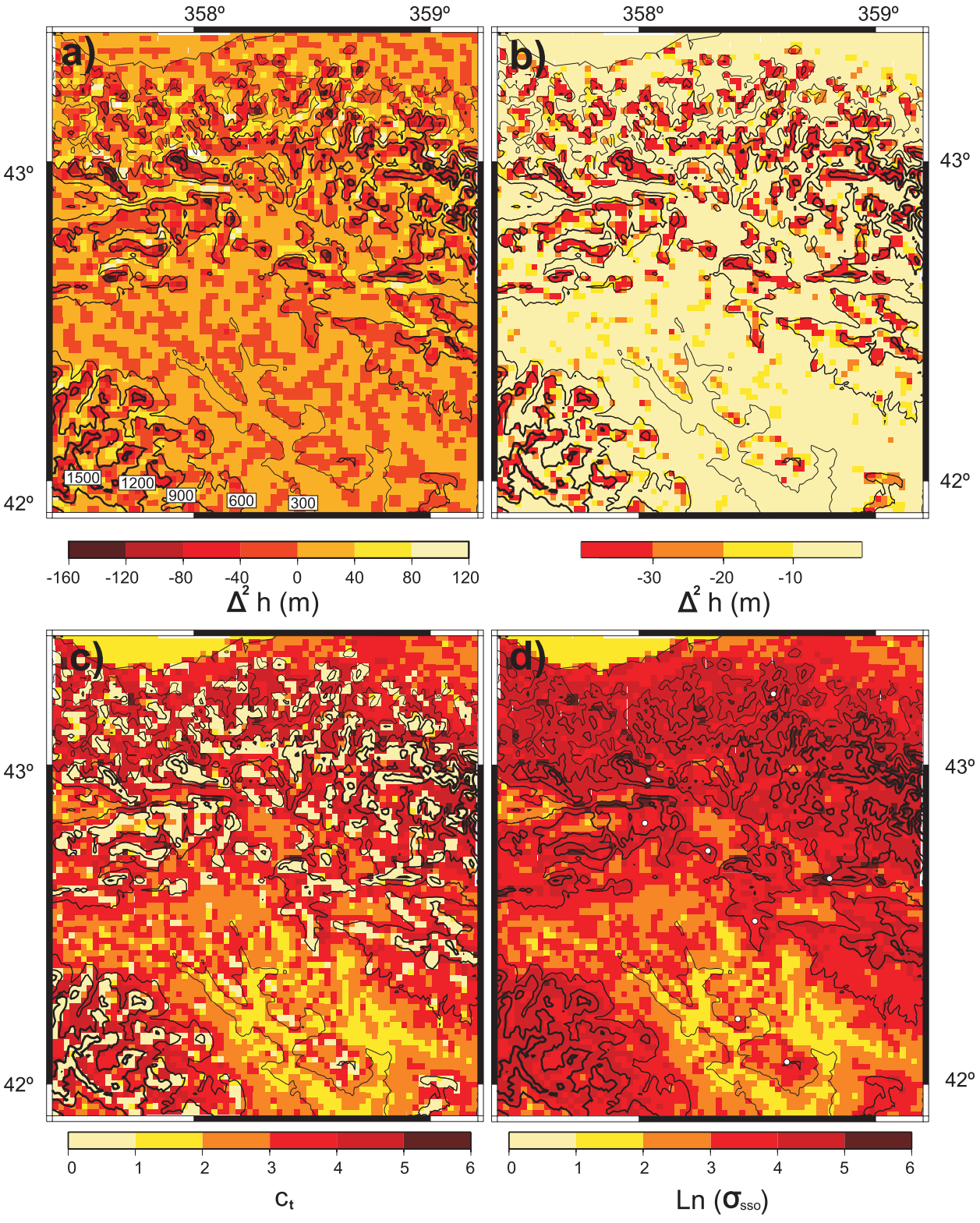


FIG. 7. Nondimensional Laplacian of the topography [Eq. (1)] over the CFN for (a),(b) the WRF domain configured at 2-km horizontal resolution, (c) $c_t$ in Eq. (2), and (d) $\ln\sigma_{sso}$. The different scales in (a) and (b) are introduced to highlight in (b) the different topographic regions used in the parameterization. The contour lines represent the topography, and the circles in (d) are the observational sites located over mountains or hills.

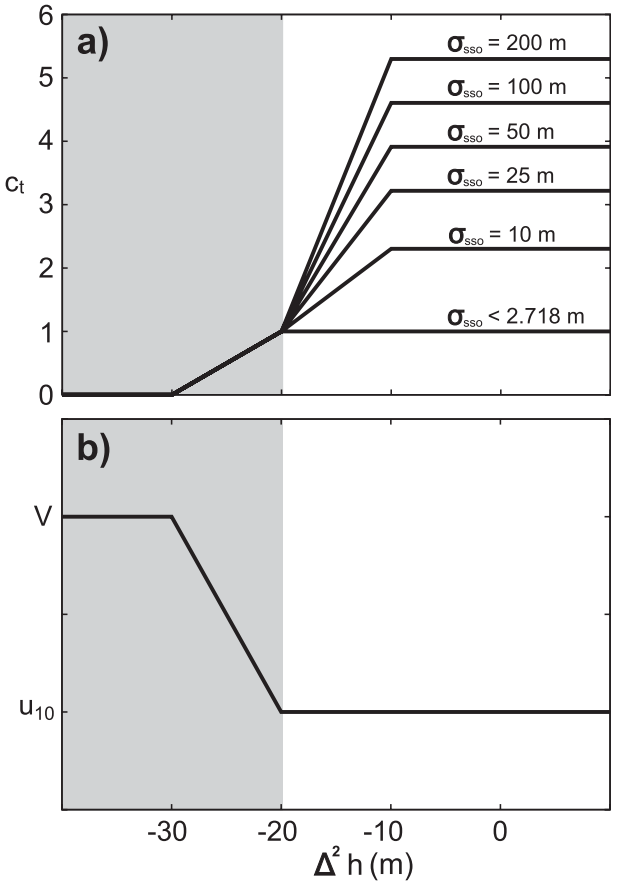


FIG. 8. (a) Factor $c_t$ as a function of $\Delta^2 h$ and $\sigma_{sso}$. (b) The surface wind as a function of $\Delta^2 h$. The gray-shaded area highlights the regions defined as mountainous ($\Delta^2 h < -20$ m).

and its related discussion). A gradual weighting of the 10-m wind diagnostic $u_{10}$ toward the wind at the lowest level $V$ is also introduced at the mountains (Fig. 8b), which enhances the strength and thus partially compensates for the underestimation of the mountain height and also contributes toward highlighting the upstream influence that decouples the wind from the ground. In particular, $u_{10} = \alpha_2 u_{10} + (1 - \alpha_2)V$, where $\alpha_2 = (\Delta^2 h + 30)/10$.

The $\ln\sigma_{sso}$ term operates in the plains and valleys and is designed to correct for the higher biases seen where subgrid terrain is more complex; therefore, in these regions $c_t$ is only dependent on the subgrid term (Fig. 8a). The logarithm is used to provide reasonable values of $c_t$ for the wide range of potential values of $\sigma_{sso}$, which is near zero over the plains and is up to 200 m over the most-complex areas (Fig. 4). In intermediate regions ($-20 > \Delta^2 h > -10$), $c_t$ makes a transition from a function of only $\Delta^2 h$ to a function of only $\ln\sigma_{sso}$ by using a weighted function of both. Notice that $c_t$ is not allowed to become smaller than 1 over the plains/valleys ($c_t = 1$ if $\sigma_{sso} < e$). This condition is imposed to avoid a smaller surface drag term than the one from the default WRF formulation wherein $c_t$ is always 1.

The spatial distribution of $c_t$ over the CFN is shown in Fig. 7c. It ranges from 0 to 6 and thus does not show inordinately high values that would be indicative of an unrealistic drag. It is interesting to compare it with the subgrid term $\ln\sigma_{sso}$ (Fig. 7d). The mountain sites show 0 values of $c_t$ that would help to mitigate the low bias found at these sites. On the contrary, $\ln\sigma_{sso}$ shows high values that would produce an even worse WRF performance at the mountainous sites. This comparison clearly shows the strength of combining information about the resolved terrain $\Delta^2 h$ and the subgrid information $\ln\sigma_{sso}$ and indicates that a parameterization of the unresolved topography should not be based only on subgrid information.

## 4. Description of the numerical experiment

The parameterization of subgrid-scale orography was tested using the WRF model, version 3.1.1 (Skamarock et al. 2008). The winter of 2001/02 (December–February) has been simulated using the default WRF (WRFref hereinafter) and introducing the parameterization described in the previous section (WRFnew). The investigation focuses on winter to mitigate the influence of thermally driven circulations, which are more important in summer, and thus to concentrate on the interaction of the large scale with the topographic features. The same dynamical settings used by JEA10 have been adopted herein. The WRF model is basically configured with a total of four domains, interacting in two-way nesting, to progressively reach 2 km of horizontal resolution over the CFN. A total of 31 $\eta$ levels are used in the vertical direction.

Standard physical options also in concordance with the JEA10 simulation are used. The shortwave radiation is parameterized as in Dudhia (1989) whereas the Rapid Radiative Transfer Model is used for the longwave radiation (Mlawer et al. 1997). The cumuli are parameterized in the three outermost domains following the approach of Kain and Fritsch (1990, 1993), whereas the microphysics scheme adopted, the WRF single-moment six-class method, follows Hong and Lim (2006). A simple land surface model that is based on the fifth-generation Pennsylvania State University–National Center for Atmospheric Research Mesoscale Model (MM5) five-layer soil temperature model is used (Dudhia 1996; Dudhia et al. 2004). The Yonsei University scheme has been used to parameterize the planetary boundary layer processes (Hong et al. 2006), being the part of the code wherein the parameterization of the unresolved drag described

in the previous section has been implemented. For more details on the physical and dynamical settings, the interested reader is referred to JEA10 and Skamarock et al. (2008).

The strategy used in the numerical simulations also follows JEA10. Each WRF simulation (WRFref and WRFnew) consists of a sequence of short WRF runs. The WRF model is initialized at 0000 UTC of a given day and is run for 48 simulated h, storing the output every hour. The first day of the simulation is discarded as a spinup of the model, and the values for the following 24 h are retained as the simulation for that day. The process is repeated until a simulation for all of the winter-2002 days is obtained. Data from the operational analysis performed every 6 h at 1° horizontal resolution at the National Centers for Environmental Prediction (NCEP final analysis) are used as initial and boundary conditions for the simulations.

## 5. Results

The results are organized into two sections. Section 5a compares the performance of WRFref and WRFnew using the simulated wind at the nearest grid points with the observational sites. Section 5b shows the problems associated with *representativeness errors* and how the selection of more-representative grid points than the nearest ones is able to improve the model evaluation.

### *a. Performance of the new parameterization*

The wind speed bias calculated with WRFref is displayed in Fig. 9a. The simulated wind at the nearest grid point to the observational sites is used in the comparison. A similar pattern to the bias obtained with the >13-yr simulation performed by JEA10 can be appreciated (Fig. 3a). The wind speed is overestimated over the plains and valleys and underestimated at the mountains and hills (Fig. 9a). Hence, the season selected for the experiment, the winter of 2002, can be considered to be representative of the default WRF performance.

The WRF simulation that takes into account the effects of the unresolved terrain, WRFnew, reduces the wind speed biases at most of the observational sites (Fig. 9b). It shows near-zero biases at many places, including locations in the plains (stations 1, 13, 17, 32, and 33), over the valleys to the south of the Pyrenees (stations 10, 27, and 41), and even in the more-complex valleys of the north (15 and 22). Perhaps as interesting as the fact that the biases are small at most of the sites is that there is not a systematic high wind speed bias. The wind speed is still overestimated at certain locations (e.g., stations 2, 9, and 22) but is underestimated at other sites (e.g., 18, 25, and 27). Results for the hills and mountains also show a general improvement when WRFnew is used. For instance, station 35 located at the top of a mountain shows a reduction of the bias from $-2.35$ to $-0.22$ m s$^{-1}$, and station 8 located on a hill shows an almost complete suppression of its bias ($+0.004$ m s$^{-1}$). There is still a clear tendency to underestimate the wind speed at these mountainous locations (Fig. 9b), however.

Model performance as a function of $\Delta^2 h$ and of $\sigma_{\rm sso}$, the parameters of the scheme, is shown in Figs. 10a and 10b for WRFref and WRFnew, respectively. The parameterization reduces the high bias not only for stations located in the less-complex plains/valleys wherein most of the stations are located ($\sigma_{\rm sso} < 100$ m) but also for the two sites showing the most-complicated terrain variations ($\sigma_{\rm sso} > 100$ m). The reduction of the bias at the hills and mountains ($\Delta^2 h < -20$ m) of different complexity is also evident, but in these cases there is still a clear tendency to underestimate the wind speed, especially at the steepest peaks ($\sigma_{\rm sso} > 100$ m).

Despite the improvements shown by WRFnew, there are still a couple of stations (21 and 38) that show remarkably poor performance when the new scheme is used (see Figs. 9a and 9b). These and other stations to a lesser extent are affected by representativeness errors. The nearest grid point is not the most appropriate to represent the location of the observational site; rather, nearby grid points are better suited for this purpose (JEA10).

### *b. Representativeness errors*

Representative examples of this kind of problem are shown in Fig. 11. The topography around station 21 calculated with the dataset of 90-m resolution and the topography used in the WRF simulation (2 km) are shown in Figs. 11a and 11b, respectively. The station is located on the western side of a hill, but the smoother orography used in WRF places the station on the top of the hill. A more representative location would be the nearby grid point located on the foothill and highlighted with an arrow in Fig. 11b. A similar representativeness error affects station 38 (Figs. 11c,d). The station is located in a small valley on a mesa, with a sharp terrain elevation to the north (Fig. 11c). Again, the station is located on the top of the terrain feature in WRF, and a nearby grid point (highlighted in Fig. 11d) can be considered to be more representative of the terrain characteristics of the site. In both cases (stations 21 and 38), the use of the nearest grid point erroneously located the stations on top of hills, which could be the reason for the overestimation of the wind at these sites by WRFnew (Fig. 9b).

Another kind of representativeness error affects station 40 (Figs. 11e,f). The error in this case is associated

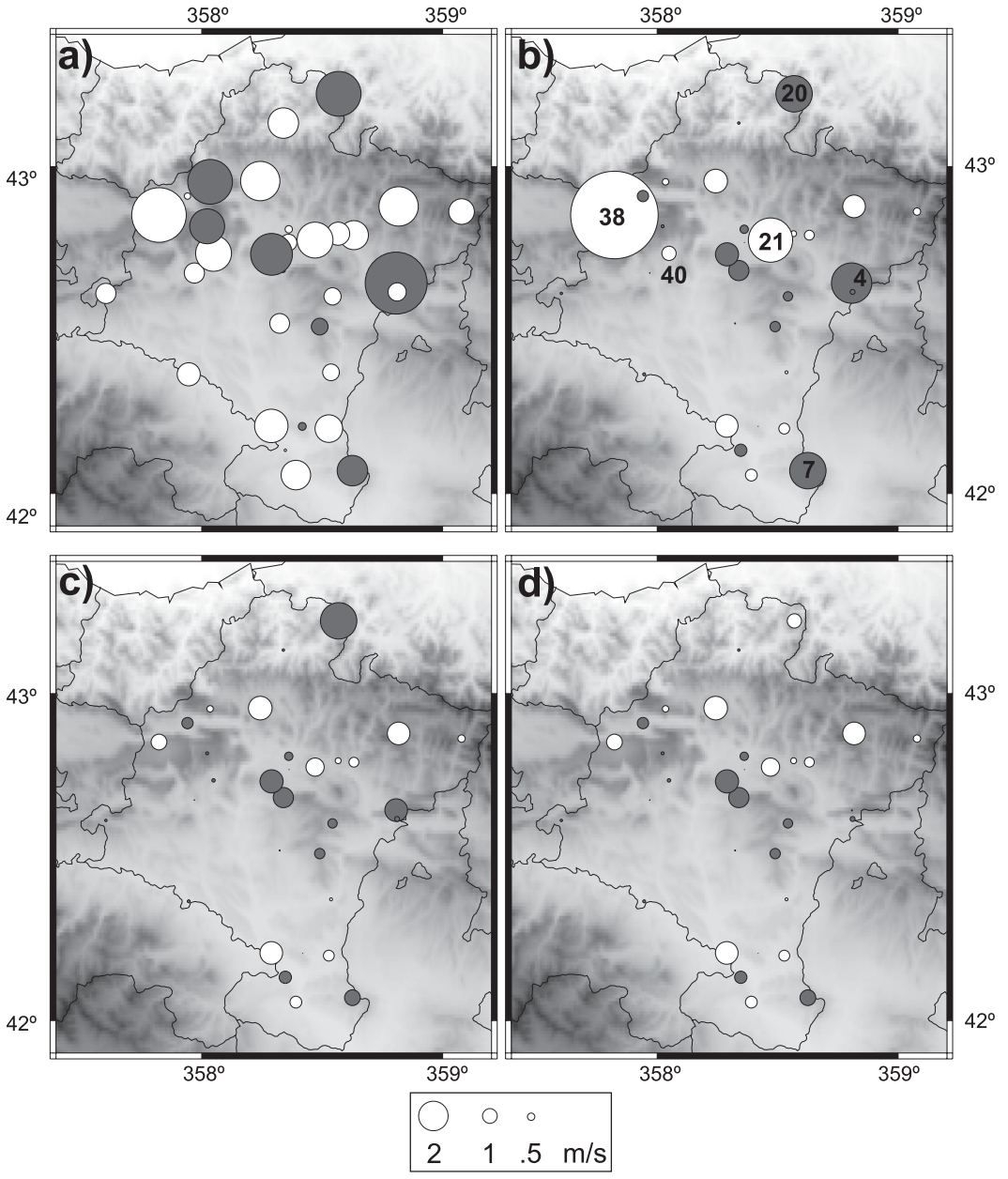


FIG. 9. Wind speed bias of (a) WRFref, (b) WRFnew, (c) WRFnew using representative grid points in the horizontal direction, and (d) WRFnew using representative grid points in the horizontal and vertical directions. A white (gray) circle denotes a wind speed overestimation (underestimation). The numbers in (b) represent the codes of the stations that suffer from representativeness errors.

with the characteristics of the surface physical properties. The use of the nearest grid point places the station over a body of water (the reservoir of Alloz; Fig. 11f) instead of over land. The $z_0$ is smaller over bodies of water than it is over land, and thus this representativeness error would produce an erroneously high flow speed at this site. Indeed, the WRFnew simulation shows a high wind speed bias at this site (Fig. 9b). A better choice to represent the surface physical properties of the location would be to use a nearby grid point located on the shore, such as the grid point highlighted in Fig. 11f.

A total of five stations were affected by representativeness errors. The above-mentioned stations 21, 38, and 40; station 7, which is located on the top of a hill but is represented on the slope by WRF; and station 4, which is situated on the top of a steep mountain whereas a

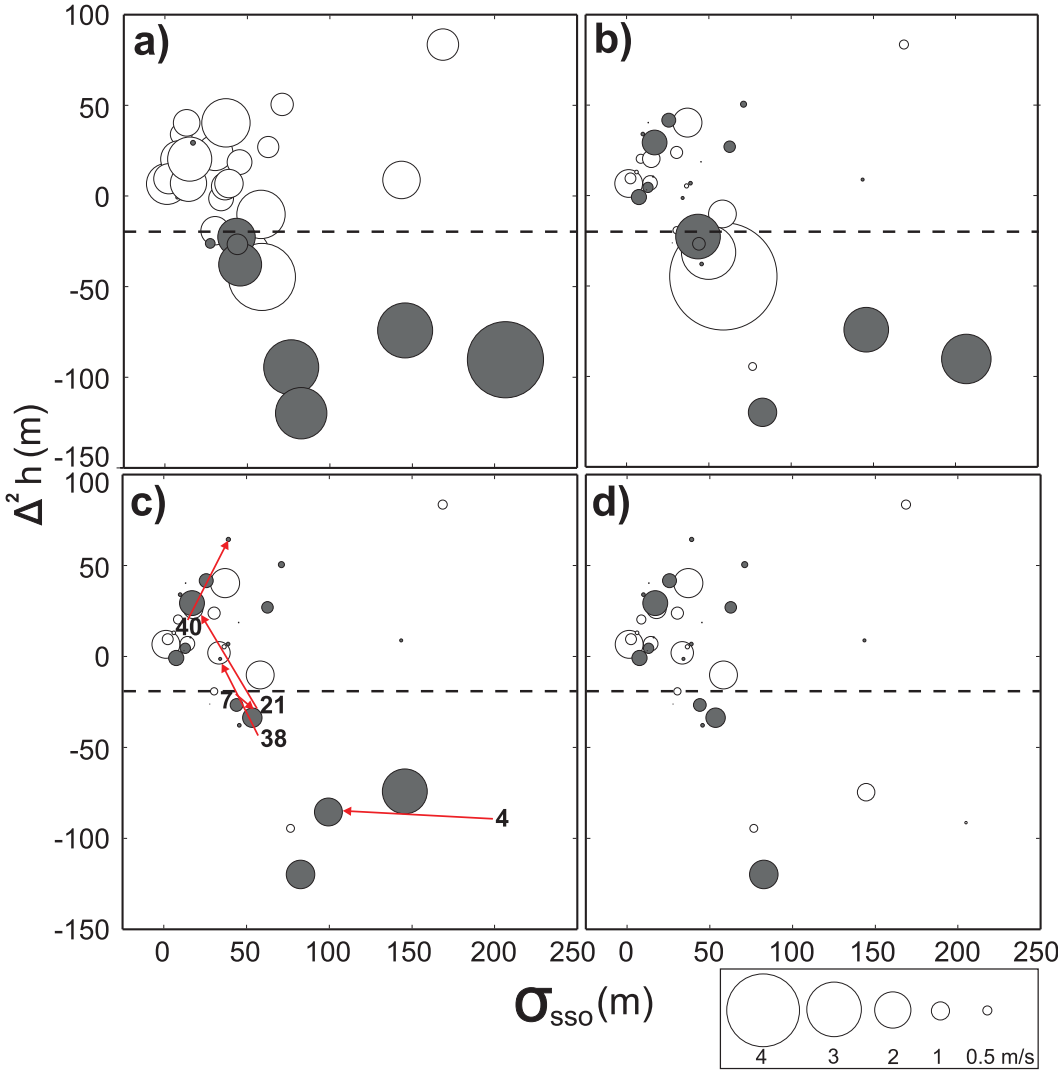


FIG. 10. Wind speed bias (circles) as a function of $\Delta^2 h$ and $\sigma_{sso}$ for (a) WRFref, (b) WRFnew, (c) WRFnew using representative grid points in the horizontal direction, and (d) WRFnew using representative grid points in the horizontal and vertical directions. A white (gray) circle denotes a wind speed overestimation (underestimation). The dashed lines highlight $\Delta^2 h$ values of −20 m. The arrows in (c) highlight the change associated with the use of nearby grid points that are more appropriate for avoiding representativeness errors (the numbers denote the codes of the stations).

closer and steeper nearby grid point would be more appropriate. The wind speed bias as a result of using representative grid points in the WRFnew simulation is shown in Figs. 9c and 10c. The five cases show a better wind speed estimation using the representative grid points instead of the nearest grid points. In particular, the two stations that showed the worst performance (21 and 38; see Fig. 9b) now show large reductions in bias: 1.76 and 4.85 m $s^{-1}$, respectively.

Despite the better WRF performance as a consequence of introducing the new parameterization and selecting representative grid points (Fig. 10c), there is still a clear tendency to underestimate the wind at the hills and mountains ($\Delta^2 h < -20$ m), especially over the steepest ones (say, $\Delta^2 h < -50$ m). Let the discussion return for a moment to the WRFnew evaluation using the nearest grid points and thus the volumes that enclose the actual location of the stations (Fig. 10b). The steepest mountains ($\Delta^2 h < -50$ m) show a tendency to overestimate the wind, especially those areas that also show a high standard deviation of the unresolved terrain ($\sigma_{sso} >$ 100 m): stations 4 and 20. The low $\Delta^2 h$ and the high $\sigma_{sso}$ indicate a steep resolved mountain with a sharp unresolved peak since the model largely underestimates

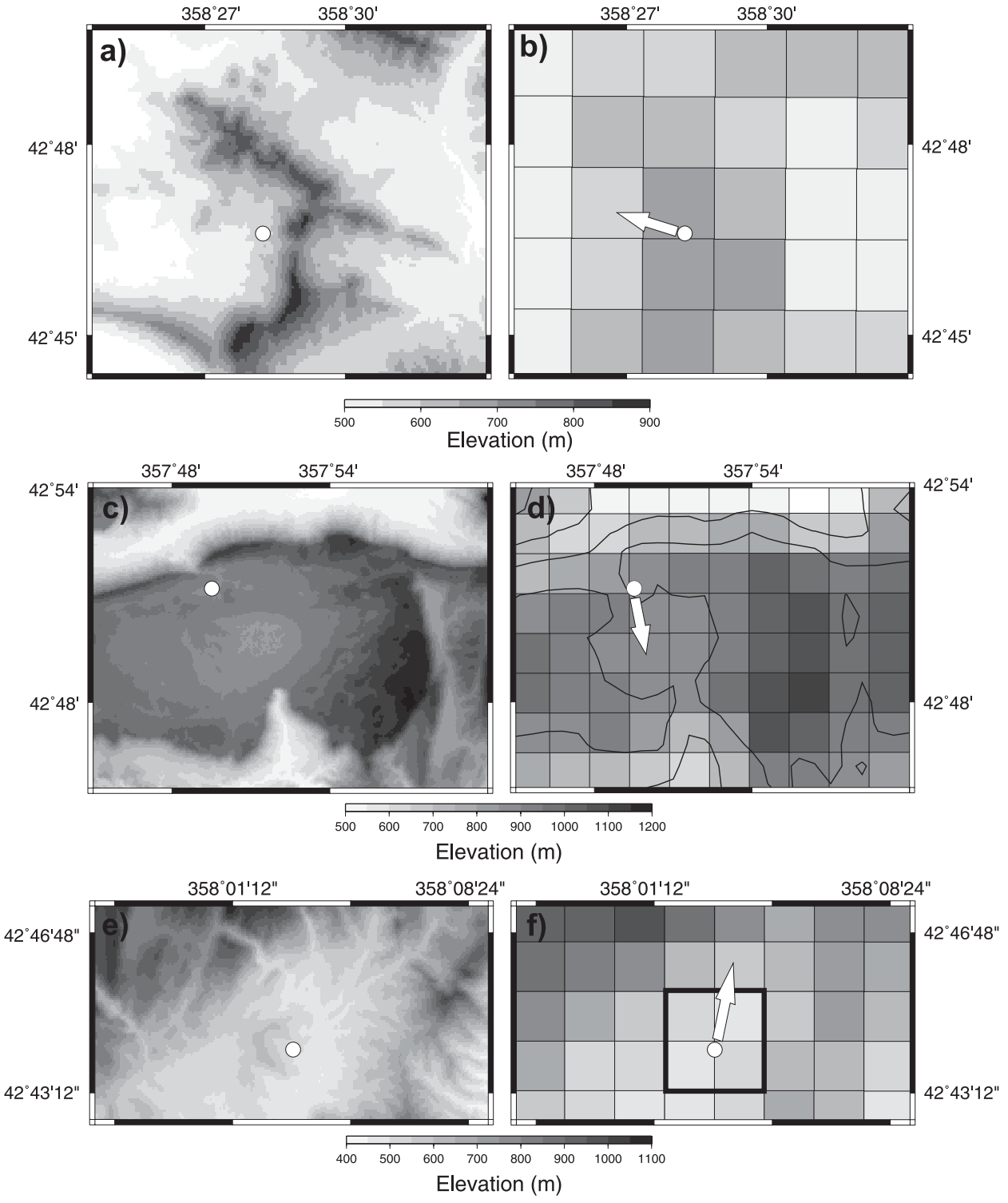


FIG. 11. Topography calculated with (left) the high-resolution dataset and (right) the WRF model configured at 2 km. The panels highlight the locations of stations (top) 21, (middle) 38, and (bottom) 40. Circles represent the stations, whereas arrows indicate more-representative grid cells. The thick rectangle in (f) highlights the location of a body of water in the WRF model, and the contour lines in (d) represent the topography.

the mountains' height (521 and 371 m at stations 4 and 20, respectively). It could be argued that these sites are well exposed to the large-scale wind and thus in a certain way are decoupled from the surface effects (see section 2b). Hence, the grid point at the true elevation of the station could be argued to be more representative than the wind at 10 m above the model surface. The effects that this change produces in the model evaluation are shown in Figs. 9d and 10d. The bias is almost absent at station 4 (0.12 m $s^{-1}$), and it is largely reduced at station 20 (from −3.04 to 0.96 m $s^{-1}$). Hence, the most representative grid points not only can be found in the horizontal direction; nearby grid points in the vertical direction should also be considered. Note also that the systematic low bias at the mountainous areas ($\Delta^2 h < -20$ m) has been practically suppressed since stations at these locations present both an overestimation and underestimation of the wind (Fig. 10d).

The changes introduced with the parameterization and the selection of representative grid points also allow improvement of the diurnal wind evolution at the mountain locations. These areas presented an opposite diurnal evolution to that observed (e.g., Fig. 6). The wind speed diurnal cycle calculated with the observations and the simulations (WRFref and WRFnew) for two mountain stations (20 and 3) is shown in Fig. 12. The first station combines the use of the parameterization and the selection of a more representative grid point in the vertical direction, whereas in the second case only the effects of the parameterization are shown since the nearest grid point is the most representative at this site. WRFref shows both a better estimation of the mean wind and a diurnal evolution that is more in agreement with the observed behavior.

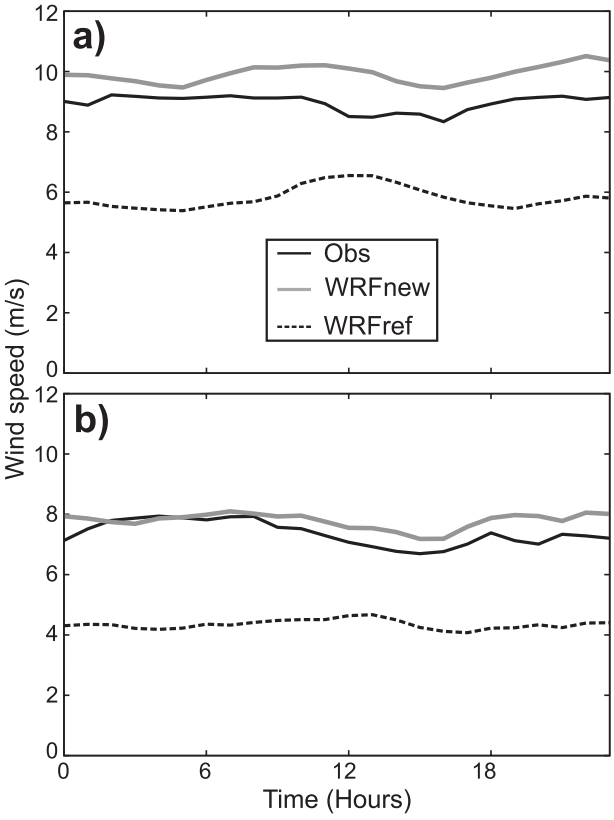


FIG. 12. Wind speed diurnal cycle at stations (a) 20 and (b) 3, as a result of averaging the observations (black solid line) as well as the simulated wind from WRFnew (gray solid line) and WRFref (dashed line).

## 6. Summary, discussion, and conclusions

A new scheme to parameterize the effects that the unresolved topography exerts over the surface circulations has been implemented in WRF. The scheme uses a new surface sink term in the momentum equation to take into account the effects of the unresolved terrain features and thus avoid the problems associated with the use of an effective roughness length (Wood et al. 2001; Beljaars et al. 2004). A WRF simulation using the proposed scheme outperforms the surface wind estimations obtained with the default WRF simulation over a complex-terrain region located in the northeast of the Iberian Peninsula. In particular, the scheme corrects the high wind speed bias over the plains and valleys reported in previous works (e.g., Cheng and Steenburgh 2005; Bernardet et al. 2005; Roux et al. 2009; Mass and Ovens 2010, 2011). The proposed parameterization also improves the wind estimations over hills and mountains where it has been shown that the WRF model presented a low bias. The correction of both systematic biases allowed improvement of the underestimation of the spatial wind variability that the default WRF shows.

The importance of selecting representative grid points for evaluating the model performance has been shown to be of particular relevance. For instance, station 38 showed a reduction of the bias of 4.85 m $s^{-1}$ just by selecting a more representative grid point. The most appropriate grid points can be found at nearby horizontal grid cells but also in the vertical direction. Caution must be taken if the points for comparison are selected on the basis of the nearest Euclidean distance or some kind of weighting of the same.

The inclusion of the parameterization and an appropriate selection of representative grid points reduce the mean absolute error of the mean wind speed estimations from 1.85 to 0.72 m $s^{-1}$. In view of the improved model performance, which not only shows small biases but also reveals the absence of any systematic behavior over the plains/valleys or hills/mountains (Figs. 9d and 10d), one

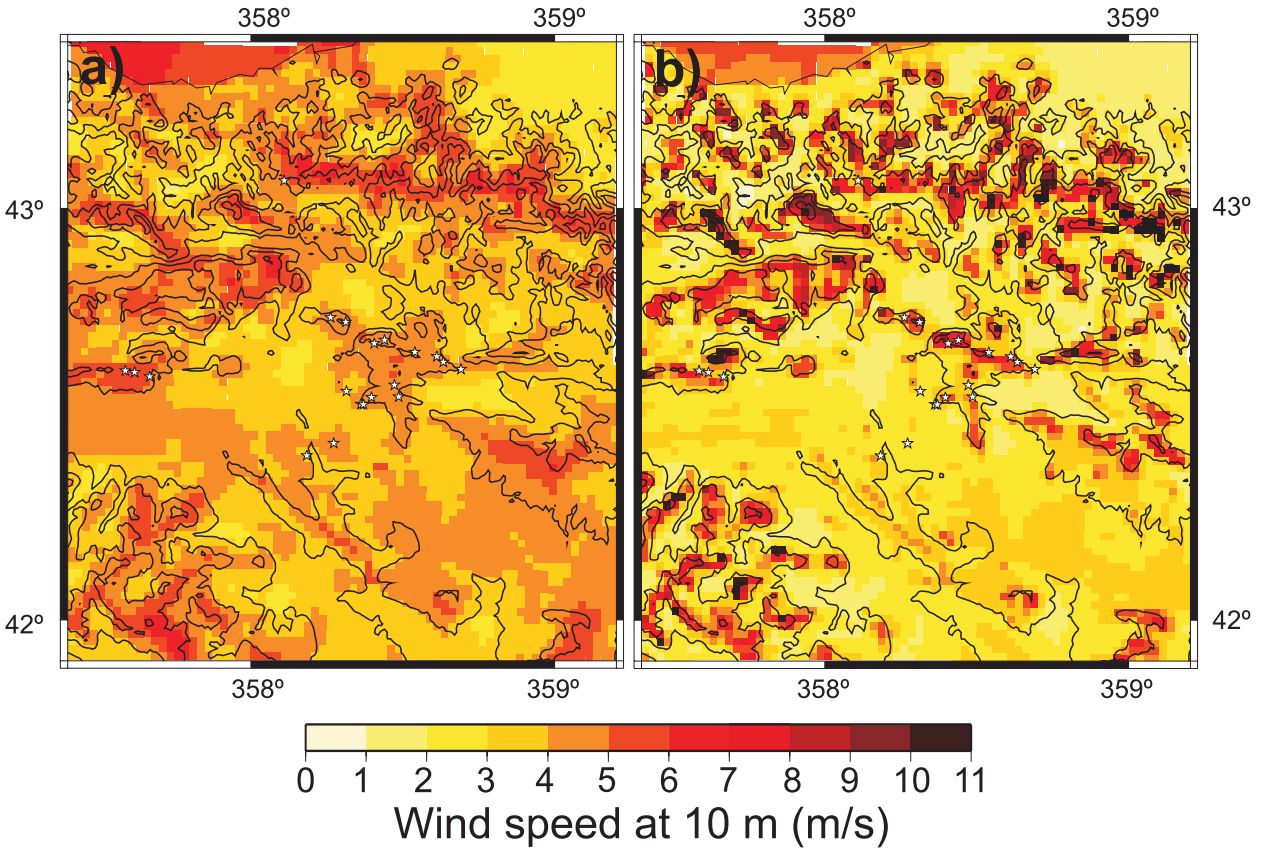


FIG. 13. Wind speed at 10 m above ground level calculated with (a) WRFref and (b) WRFnew. WRFnew uses the wind speed at the elevation of the maximum height of the subgrid-scale orography to represent the wind speeds at those grid cells with $\Delta^2 h < -50$ m and $\sigma_{sso} > 100$ m. Stars indicate locations of wind farms.

has more confidence in using the simulation to infer the wind speed at those sites where no wind observations are available. An improved climatological description of the surface wind is not only useful from an academic point of view but is of relevance for numerous applications such as the transport and dispersion of pollutants over a region, the analysis of extreme wind speed for insurance companies, or wind resource evaluation. The potential benefits that the new scheme can produce for these kinds of applications are further illustrated for the case of wind-resource evaluation.

The CFN has strong wind conditions, which has allowed for the spread of wind energy facilities during the last two decades (Fairless 2007; García-Bustamante et al. 2008, 2009). Figure 13 shows the mean wind speed from WRFref and WRFnew and the location of some wind farms (stars). The reduced spatial variability of WRFref (Fig. 13a) in comparison with WRFnew (Fig. 13b) is evident. The reduced variability makes it harder to identify the most appropriate locations (the windiest ones) from those not so well suited for wind-energy exploitation. Although the wind farms are located over reasonably windy areas (Fig. 13a), there are other areas that seem just as windy as these ones (e.g., the plains in the south, the coastal areas of the north, and the mountainous areas of the Pyrenees). Some of these areas would be more appropriate than the selected locations (stars) since access to them is easier.

The climatological winds calculated with WRFnew narrow down the potential locations for the installation of wind-energy farms (Fig. 13b). Many places in the southern plains no longer show a large wind potential; the coastal areas show a reduced wind speed, as do many valleys in the Pyrenees. The already-installed wind farms tend to be located near grid points of high wind resource and it becomes more understandable why these sites are selected for wind-energy exploitation. This constitutes an indirect confirmation of the benefits provided by the parameterization if we assume that the already-installed wind farms are located in appropriate places. A more detailed evaluation of the parameterization performance, including the simulation of a complete year, would be desirable before using the scheme for routine wind-energy applications. Preliminary results showed that

the corrections also reduced the modeled wind biases for the summer.

The new scheme not only contributes to an improved climatological wind description but also produces a diurnal wind speed cycle that is more in phase with the observed wind at the mountain sites. This is an important achievement if we take into account the extreme location of these sites, which are poorly reproduced even though a high horizontal resolution of 2 km is used. Mountain sites have rarely been evaluated before, and this study shows how biases may be reduced there. The scheme should be tested in the future during other seasons to confirm the adequacy of the underlying physical ideas.

Despite the improvements shown in the wind speed estimations over the CFN, the parameterization should be tested in other areas. The use of microscale models can be helpful for increasing our understanding of the effects produced by the unresolved topography over the resolved flow. For instance, it could be useful to improve the representation of the effects produced by hills that are not usually well represented even at a horizontal resolution of a few kilometers. In addition, the scheme is believed to be independent of the horizontal resolution used, but testing the scheme at different resolutions than the one used herein (2 km) would be desirable. These kinds of analysis could eventually lead to improvements in the formulation proposed herein, which would have a positive feedback for continuing improvement of the surface wind simulation provided by the WRF model.

*Acknowledgments.* The work was supported by Projects CGL-2008-05093/CLI and CGL-2011-29677-C02 and was accomplished within Collaboration Agreement 09/490 between CIEMAT and the National Center for Atmospheric Research (NCAR). We thank the Navarra government and CIAT for facilitating the access to their datasets. The final NCEP analyses are from the Research Data Archive available at NCAR (online at http://dss.ucar.edu/datasets/ds083.2/). Special thanks are given to the PALMA research group for fruitful discussions. We also thank the reviewers for their helpful comments and Mindi E. McDonald for her careful revision of the manuscript.

## REFERENCES

Beljaars, A. C. M., A. R. Brown, and N. Wood, 2004: A new parametrization of turbulent orographic form drag. *Quart. J. Roy. Meteor. Soc.,* **130,** 1327–1347.

Bernardet, L. R., L. Nance, H.-Y. Chuang, A. Loughe, M. Demirtas, S. Koch, and R. Gall, 2005: The developmental testbed center winter forecasting experiment. Preprints, *21st Conf. on Weather Analysis and Forecasting/17th Conf. on Numerical Weather Prediction,* Washington, DC, Amer. Meteor. Soc., 7.1. [Available online at http://ams.confex.com/ams/pdfpapers/94730.pdf.]

Brown, A. R., and N. Wood, 2001: Turbulent form drag on anisotropic three-dimensional orography. *Bound.-Layer Meteor.,* **101,** 229–241.

Cheng, W. Y. Y., and W. J. Steenburgh, 2005: Evaluation of surface sensible weather forecast by the WRF and the Eta Models over the western United States. *Wea. Forecasting,* **20,** 812–821.

Chien, F.-C., and C. F. Mass, 1994: A numerical study of the interaction between frontal systems and coastal mountains. *Proc. Fourth PSU/NCAR Mesoscale Model Users' Workshop,* Boulder, CO, NCAR, 78–82.

Dudhia, J., 1989: Numerical study of convection observed during the Winter Monsoon Experiment using a mesoscale two-dimensional model. *J. Atmos. Sci.,* **46,** 3077–3107.

——, 1996: A multilayer soil temperature model for MM5. Preprints, *Sixth PSU/NCAR Mesoscale Model Users' Workshop,* Boulder, CO, NCAR, 49–50.

——, D. Gill, K. Manning, W. Wang, and C. Bruyere, 2004: PSU/NCAR Mesoscale Modeling System tutorial class notes and user's guide (MM5 modeling system version 3). [Available online at http://www.mmm.ucar.edu/mm5/documents/tutorial-v3-notes.html.]

Fairless, D., 2007: How did a little Spanish province become one of the world's wind-energy giants? *Nature,* **447,** 1046–1048.

Farr, T. G., and Coauthors, 2007: The shuttle radar topography mission. *Rev. Geophys.,* **45,** RG2004, doi:10.1029/2005RG000183.

Fiedler, F., and H. A. Panofsky, 1972: The geostrophic drag coefficient and the 'effective' roughness length. *Quart. J. Roy. Meteor. Soc.,* **98,** 213–220.

García-Bustamante, E., J. F. González-Rouco, P. A. Jiménez, J. Navarro, and J. P. Montávez, 2008: The influence of the Weibull assumption in monthly wind energy estimation. *Wind Energy,* **11,** 483–502.

——, ——, ——, ——, and ——, 2009: A comparison of methodologies for monthly wind energy estimations. *Wind Energy,* **12,** 640–659.

——, ——, J. Navarro, E. Xoplaki, P. A. Jiménez, and J. P. Montávez, 2012: North Atlantic atmospheric circulation and surface wind in the northeast of the Iberian Peninsula: Uncertainty and long term downscaled variability. *Climate Dyn.,* **38,** 141–160.

Georgelin, M., and Coauthors, 2000: The second COMPARE exercise: A model intercomparison using a case of a typical mesoscale orographic flow, the PYREX IOP3. *Quart. J. Roy. Meteor. Soc.,* **126,** 991–1029.

Grant, A., and P. Mason, 1990: Observations of boundary-layer structure over complex terrain. *Quart. J. Roy. Meteor. Soc.,* **116,** 159–186.

Hong, S.-Y., and J.-O. J. Lim, 2006: The WRF single-moment 6-class microphysics scheme (WSM6). *J. Kor. Meteor. Soc.,* **42,** 129–151.

——, Y. Noh, and J. Dudhia, 2006: A new vertical diffusion package with an explicit treatment of entrainment processes. *Mon. Wea. Rev.,* **134,** 2318–2341.

Howard, T., and P. Clark, 2007: Correction and downscaling of NWP wind speed forecasts. *Meteor. Atmos. Phys.,* **14,** 105–116.

Jiménez, P. A., J. F. González-Rouco, J. P. Montávez, J. Navarro, E. García-Bustamante, and F. Valero, 2008: Surface wind regionalization in complex terrain. *J. Appl. Meteor. Climatol.,* **47,** 308–325.

——, ——, ——, E. García-Bustamante, and J. Navarro, 2009a: Climatology of wind patterns in the northeast of the Iberian Peninsula. *Int. J. Climatol.,* **29,** 501–525.

——, J. P. Montávez, E. García-Bustamante, J. Navarro, J. M. Jiménez-Gutiérrez, E. E. Lucio-Eceiza, and J. F. González-Rouco, 2009b: Diurnal surface wind variations over complex terrain. *Fís. Tierra,* **21,** 79–91.

——, J. F. González-Rouco, E. García-Bustamante, J. Navarro, J. P. Montávez, J. Vilà-Guerau de Arellano, J. Dudhia, and A. Roldán, 2010a: Surface wind regionalization over complex terrain: Evaluation and analysis of a high-resolution WRF numerical simulation. *J. Appl. Meteor. Climatol.,* **49,** 268–287.

——, ——, J. Navarro, J. P. Montávez, and E. García-Bustamante, 2010b: Quality assurance of surface wind observations from automated weather stations. *J. Atmos. Oceanic Technol.,* **27,** 1101–1122.

——, J. Vilà-Guerau de Arellano, J. F. González-Rouco, J. Navarro, J. P. Montávez, E. García-Bustamante, and J. Dudhia, 2011: The effect of heat waves and drought on the surface wind circulations in the northeast of the Iberian Peninsula during the summer of 2003. *J. Climate,* **24,** 5416–5422.

Kain, J. S., and J. M. Fritsch, 1990: A one-dimensional entraining/detraining plume model and its application in convective parameterization. *J. Atmos. Sci.,* **47,** 2784–2802.

——, and ——, 1993: Convective parameterization for mesoscale models: The Kain–Fritsch scheme. *The Representation of Cumulus Convection in Numerical Models, Meteor. Monogr.,* No. 46, Amer. Meteor. Soc., 165–170.

Mass, C., and D. Ovens, 2010: WRF model physics: Problems, solutions and a new paradigm for progress. Preprints, *2010 WRF Users' Workshop,* Boulder, CO, NCAR. [Available online at http://www.mmm.ucar.edu/wrf/users/workshops/WS2010/presentations/session%204/4-1_WRFworkshop2010Final.pdf.]

——, and ——, 2011: Fixing WRF's high speed wind bias: A new subgrid scale drag parameterization and the role of detailed verification. Preprints, *24th Conf. on Weather and Forecasting/20th Conf. on Numerical Weather Prediction,* Seattle, WA, Amer. Meteor. Soc., 9B.6. [Available online at http://ams.confex.com/ams/91Annual/webprogram/Paper180011.html.]

Mesinger, F., R. L. Wobus, and M. E. Baldwin, 1996: Parameterization of form drag in the Eta Model at the National Centers for Environmental Prediction. Preprints, *11th Conf. on Numerical Weather Predition,* Norfolk, VA, Amer. Meteor. Soc., 324–326.

Milton, S. F., and C. A. Wilson, 1996: The impact of parameterized subgrid-scale orographic forcing on systematic errors in a global NWP model. *Mon. Wea. Rev.,* **124,** 2023–2045.

Mlawer, E. J., S. J. Taubman, P. D. Brown, M. J. Iacono, and S. A. Clough, 1997: Radiative transfer for inhomogeneous atmospheres: RRTM, a validated correlated-*k* model for the longwave. *J. Geophys. Res.,* **102,** 16 663–16 682.

Reuter, H. I., A. Nelson, and A. Jarvis, 2007: An evaluation of void filling interpolation methods for SRTM data. *Int. J. Geogr. Inf. Sci.,* **21,** 983–1008.

Rife, D., C. Davis, and J. Knievel, 2009: Temporal changes in wind as objects for evaluating mesoscale numerical weather prediction. *Wea. Forecasting,* **24,** 1374–1389.

Rontu, L., 2006: A study on parameterization of orography-related momentum fluxes in a synoptic-scale NWP model. *Tellus,* **58A,** 69–81.

Roux, G., Y. Liu, L. D. Monache, R.-S. Sheu, and T. T. Warner, 2009: Verification of high resolution WRF-RTFDDA surface forecasts over mountains and plains. Preprints, *2009 WRF Users' Workshop,* Boulder, CO, NCAR. [Available online at http://www.mmm.ucar.edu/wrf/users/workshops/WS2009/abstracts/5B-05.pdf.]

Skamarock, W. C., and Coauthors, 2008: A description of the Advanced Research WRF version 3. NCAR Tech. Rep. TN-475+STR, 113 pp.

Wilson, J. D., 2002: Representing drag on unresolved terrain as a distributed momentum sink. *J. Atmos. Sci.,* **59,** 1629–1637.

Wood, N., and P. J. Mason, 1993: The pressure force induced by neutral, turbulent flow over hills. *Quart. J. Roy. Meteor. Soc.,* **119,** 1233–1267.

——, A. Brown, and R. Hewer, 2001: Parametrizing the effects of orography on the boundary layer: An alternative to effective roughness lengths. *Quart. J. Roy. Meteor. Soc.,* **127,** 759–777.